Modeling and Inverse Compensation of Temperature-Dependent Ionic Polymer–Metal Composite Sensor Dynamics

Thomas Ganley, David L. S. Hung, Guoming Zhu, and Xiaobo Tan, *Member, IEEE*

***Abstract*—Ionic polymer–metal composites (IPMCs) have intrinsic sensing capabilities. Like many other sensing materials, however, IPMC sensors demonstrate strong temperature-dependent behaviors. In this paper, we present the first systematic studies on temperature-dependent IPMC sensing dynamics. A cantilevered IPMC beam, soaked in a water bath with controlled temperature, is excited mechanically at its tip. The empirical frequency response of the sensor, with the tip displacement as an input and the short-circuit current as an output, shows a clear dependence on the bath temperature. The sensing dynamics is modeled with a transfer function with temperature-dependent coefficients. By fitting the values of the coefficients at a set of test temperatures, we capture the temperature dependence of the coefficients with polynomial functions, which can be used to predict the sensing dynamics at other temperatures. We also investigate the inversion of the sensing dynamics, for extracting the mechanical signal given the sensor output. A stable but noncausal inversion algorithm is applied to deal with the unstable zeros of the original sensing dynamics. Inversion with finite preview time is further explored to achieve near real-time decoding of the sensor output. Experimental results with both harmonic stimuli and free vibrations have validated the effectiveness of the proposed modeling and inversion schemes for IPMC sensors under different temperatures.**

***Index Terms*—Ionic polymer–metal composite (IPMC), inverse compensation, modeling, sensors, temperature-dependent dynamics.**

I. Introduction

OVER the past decade or so, electroactive polymers (EAPs), a novel family of smart materials have received tremendous interest for their potential applications in sensing, actuation, and energy harvesting [1]. Several important examples of EAPs include ionic polymer–metal composites (IPMCs) [2], conjugated polymers [3]–[8], and dielectric elastomers [9], [10]. In particular, IPMCs are a class of soft actuation and sensing materials that hold strong promise for versatile applications because they are amenable to microfabrication [11], work in air and in various fluid media without stringent packaging requirements, require low-actuation voltages (several volts), and have minimal structural complexity in implementation as actuators and sensors.

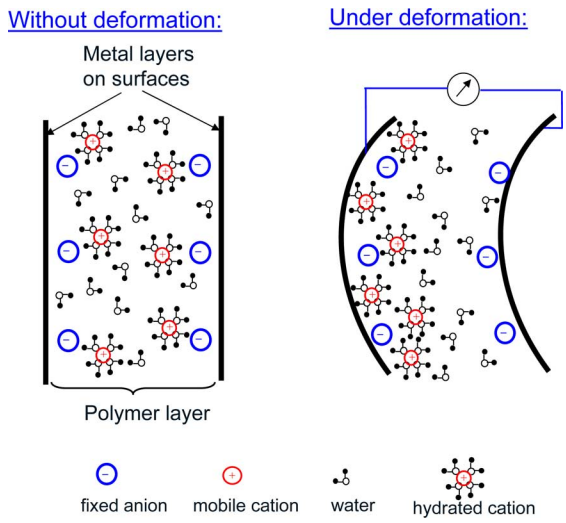

Fig. 1. Illustration of the IPMC sensing principle. A mechanical stimulus induces redistribution of mobile ions (and thus the net charge density) resulting in a detectable signal across the electrodes. Note that the illustrative schematic does not attempt to depict the ion locations precisely. In particular, in reality, fixed anions are distributed randomly throughout the ion-exchange polymer instead of being only at the proximity of the metal electrodes.

As illustrated in Fig. 1, an IPMC consists of three layers, with an ion-exchange polymer membrane (e.g., Nafion) sandwiched by metal electrodes. Inside the polymer, (negatively charged) anions covalently fixed to polymer chains are balanced by mobile (positively charged) cations. An applied voltage across an IPMC leads to the transport of cations and accompanying solvent molecules, resulting in both differential swelling and electrostatic forces inside the material, which cause the material to bend and hence the actuation effect [2], [12], [13]. IPMC actuators have been proposed for various applications in biomedical devices and underwater robotics [14]–[17]. On the other hand, an applied mechanical stimulus could redistribute the cations inside an IPMC, producing a detectable electrical signal (typically open-circuit voltage or short-circuit current) that is correlated with the mechanical stimulus (see Fig. 1), which explains the sensing principle of IPMCs. IPMC sensors have been proposed for measuring force, pressure, displacement, or velocity in medical applications, structural health monitoring, and robotics [18]–[24].

Manuscript received April 2, 2010; revised July 14, 2010; accepted October 15, 2010. Date of publication December 17, 2010; date of current version January 12, 2011. Recommended by Technical Editor G. Alici. This work was supported in part by the National Science Foundation under Grant ECCS 0547131 and in part by the Office of Naval Research under Grant N000140810640.

T. Ganley and X. Tan are with the Department of Electrical and Computer Engineering, Michigan State University, East Lansing, MI 48824 USA (e-mail: ganleyth@msu.edu; xbtan@egr.msu.edu).

D. Hung is with the University of Michigan–Shanghai Jiao Tong University Joint Institute, Shanghai 200240, China (e-mail: dhung@sjtu.edu.cn).

G. Zhu is with the Department of Mechanical Engineering, Michigan State University, East Lansing, MI 48824 USA (e-mail: zhug@egr.msu.edu).

Color versions of one or more of the figures in this paper are available online at http://ieeexplore.ieee.org.

Digital Object Identifier 10.1109/TMECH.2010.2090665

In recent years, extensive effort has been made in modeling and understanding IPMC sensors [25]. de Gennes *et al.* proposed a static model based on linear irreversible thermodynamics to capture both actuation and sensing mechanisms of IPMCs [26]. Using an analogy to piezoelectric materials, Newbury and Leo presented a geometrically scalable "gray-box" model for IPMC actuators and sensors [27], [28]. The latter model was further elaborated and verified by Bonomo *et al.* [29]. Farinholt and Leo [30] derived the charge sensing response for a cantilevered IPMC beam under a step change in tip displacement, which is based on a partial differential equation governing the charge dynamics proposed by Nemat-Nasser and Li [12]. Taking a systems perspective, Chen *et al.* developed a physics-based, geometrically scalable model for IPMC sensors, represented as an infinite-dimensional transfer function [31]. Takagi *et al.* examined the modeling of IPMC sensors using the voltage and the current as the output, respectively, and studied the influence of the cations on the sensing dynamics [32].

Despite the aforementioned progress, there has been little or no studies reported on temperature-dependent sensing behaviors of IPMCs. As for many other sensing materials, however, temperature has a significant impact on the behavior of IPMC sensors through its influence on ion/solvent transport and electrical/mechanical properties of the material. In various applications envisioned for IPMC sensors (e.g., structural health monitoring, biomedical devices), the temperature of the working environment of an IPMC sensor could vary significantly. Without properly accounting for the influence of the temperature, it will be difficult to accurately interpret the results from the IPMC sensor output.

In this paper, we present, to our best knowledge, the *first* systematic studies of the temperature dependence of IPMC sensing dynamics, including its experimental characterization, modeling, and inverse compensation. To characterize the sensor dynamics, we place a cantilevered IPMC beam in a water bath, the temperature of which can be precisely controlled. The short-circuit current output of the IPMC is measured as the beam tip is subject to harmonic excitation. The empirical frequency response of the sensor, with the tip displacement as an input and the short-circuit current as an output, exhibits a clear dependence on the bath temperature.

While one could try to capture the temperature-dependent sensing behavior using physics-based models (e.g., [31]), such an approach would be difficult since temperature influences virtually all physical parameters, including diffusivity, dielectric constant, density, Young's modulus, and electromechanical coupling. Identifying the relationships between those parameters and temperature is a daunting task. Therefore, an empirical modeling approach is adopted here, where a transfer function with temperature-dependent coefficients is used to represent the sensing dynamics. The values of the coefficients for a set of temperatures are identified by fitting the measured frequency responses at those temperatures. Through curve fitting, these values are subsequently used to obtain low-order polynomial functions that describe how individual coefficients vary with the temperature. These coefficient functions enable one to obtain the sensor model at other temperatures, as we show later in this paper.

In real applications, one is interested in extracting information about the mechanical stimuli (e.g., the displacement) based on the sensor output. This requires inverting the sensor dynamics. However, the IPMC sensing dynamics turns out to be of nonminimum phase; in other words, it has zeros with positive real parts, or "unstable" zeros. Consequently, the direct inverse of the original sensing dynamics is an unstable system and thus cannot be implemented. To address this problem, we exploit the techniques for inverting nonminimum-phase systems [33], where the resulting inverse is stable but noncausal. In particular, to obtain the sensor input at time t, the algorithm requires the output trajectory during $[t, \infty)$. To facilitate near real-time decoding of the sensor input, we further explore inverse compensation with finite preview time (i.e., look-ahead time) [34]. Experimental results with both harmonic stimuli and free vibrations have validated the effectiveness of the proposed modeling and inversion schemes for IPMC sensors under different temperatures.

The remainder of this paper is organized as follows. The characterization of the temperature-dependent IPMC sensing behavior is presented in Section II. Modeling of such a dependence is discussed in Section III. In Section IV, we describe the inverse compensation algorithm and show its effectiveness with experimental results. Inversion with finite preview time is presented in Section V. Finally, concluding remarks are provided in Section VI.

II. Experimental Characterization of Temperature-Dependent IPMC Sensing Dynamics

A. Material Preparation and Experimental Setup

The IPMC used in this study was fabricated with Nafion-117, a commercial ion-exchange material from DuPont, by following the general ion-exchange and electroless electrode plating processes described in [35]. First, oxygen and argon plasma treatment was applied to roughen the surface of the Nafion film [36], followed by cleaning with boiling acid (HCl) and then with boiling deionized water (*sample preparation*). After these preparation steps, the sample was placed in $[\mathrm{Pt}(\mathrm{NH_3})_4]\mathrm{Cl_2}$ for over 3 h to incorporate the platinum complex cations into the polymer (*ion-exchange*). Then, we applied the reducing agent $\mathrm{NaBH_4}$ to the membrane in a water bath of 60 °C, which reduced the platinum complex ions to platinum near the membrane surfaces (*electrode plating*). The ion-exchange and electrode plating processes were repeated several times until the electrodes were sufficiently strong and thick, as indicated by the surface resistance. Finally, a layer of gold (100 nm) was deposited with e-beam to further reduce the surface resistance. The final thickness of the IPMC film was about 210 μm. A sample with length 18 mm and width 6.5 mm was used in the following experiments.

Fig. 2 shows the experimental setup for characterizing the IPMC sensor dynamics at different temperatures. A cantilevered IPMC beam was soaked in a water bath sitting on a digital hotplate (Thermo Scientific, HP131225). A relay controller (Auber Instruments, SYL-2342) was used to control the bath temperature with a precision of 0.5 °C, based on the feedback from a

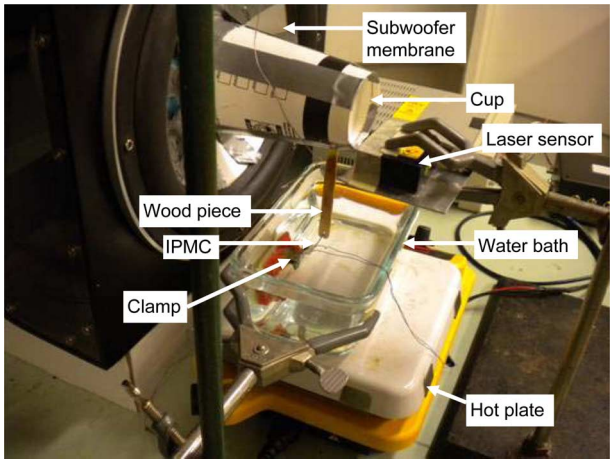

Fig. 2. Experimental setup for characterizing temperature-dependent IPMC sensing behavior.

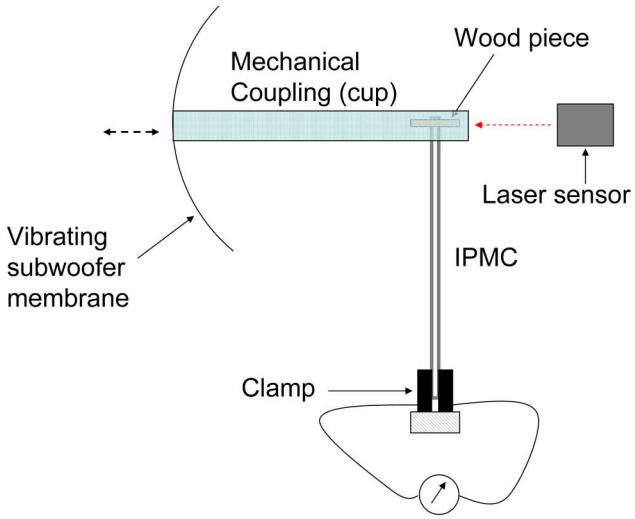

Fig. 3. Schematic of the mechanical excitation mechanism (top view).

T-type thermal couple (Omega, HTTC36-T-116G-6). For mechanical excitation, the tip of the IPMC beam was inserted into a slit cut in a wooden piece, which was firmly coupled to the membrane of a subwoofer speaker through a lightweight cup. A voltage applied to the speaker induces vibration of the membrane and, subsequently, tip displacement of the IPMC beam. The mechanical excitation mechanism is further illustrated in Fig. 3. Since the IPMC beam is very flexible and presents little resistance to the motion of the wood piece, we can treat the mechanical coupling from the speaker membrane to the IPMC tip as nearly rigid and assume that the IPMC tip displacement is identical to the displacement of the coupling cup, which was measured with a laser sensor (Baumer Electric, OADM 20I6441/S14F).

The short-circuit current measured between the two electrodes of the IPMC beam was taken as the sensor output. Fig. 4 shows the schematic of the measurement circuit, which consists of two cascaded operational amplifiers (op-amps). Since the "-" terminal of op-amp 1 is virtually the ground, the two electrodes

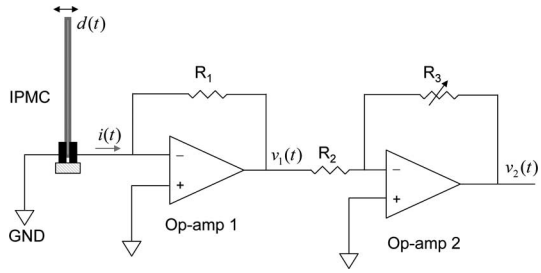

Fig. 4. Circuit for measuring the short-circuit current generated by the IPMC sensor.

of IPMC are short-circuited. The sensing current generated under this configuration $i(t)$ is proportional to the voltage output $v_1(t) = R_1 i(t)$. The second op-amp is introduced for gain adjustment, where the resistor R_3 is tunable. The output $v_2(t)$ is related to the current signal $i(t)$ via $v_2(t) = (R_3 R_1 / R_2) i(t)$. In the circuit we used, $R_1 = 470\ \text{k}\Omega$, $R_2 = 10\ \text{k}\Omega$, and R_3 was adjustable from 0 to 50 kΩ. Acquisition and processing of the IPMC sensor output and the laser sensor output were conducted through a dSPACE system (dSPACE, DS1104).

B. Characterization and Discussion of Temperature-Dependent Sensing Behavior

The IPMC sensor is treated as a dynamic system, where its input is the tip displacement $d(t)$ and its output is the short-circuit current $i(t)$. For a sinusoidal displacement, $d(t) = d_0 \sin(2\pi f t)$ with frequency f, and the corresponding current output $i(t)$ is not a pure sinusoidal signal in general, due to the electromechanical nonlinearities of the material. However, for relatively small stimuli, we can treat the sensor as approximately linear and extract the fundamental frequency component $i_0(t) = i_0(f) \sin(2\pi f t + \phi(f))$ from the measured $i(t)$, using techniques such as the fast Fourier transform. The empirical frequency response of the sensor, consisting of the gain response and the phase response, indicates how the sensor responds to the stimulus at different frequencies. In particular, the gain (or magnitude) response is defined as $M(f) = 20 \log_{10}(i_0(f)/d_0)$ and the phase response is defined as $\phi(f)$, both as a function of the frequency f. In this paper, the units of $d(t)$ and $i(t)$ are taken to be mm and μA, respectively. The magnitude M and the phase ϕ are expressed in terms of decibel and degree, respectively. These definitions will apply to Figs. 5, 8 and 9 in the following.

In our experiments, for a given temperature, a sinusoidal tip displacement was applied with frequency ranging from 10 to 100 Hz and the corresponding sensor output was recorded. IPMC could sense stimuli lower than 10 Hz [31] or higher than 100 Hz, but we had restricted to the aforementioned frequency range because of the bandwidth constraint of the speaker system. In particular, the response of the speaker becomes jerky when the frequency of the input is lower than 10 Hz, and becomes weak when the frequency is higher than 100 Hz, which is understandable considering its original intended use. However, as we will further discuss in Section VI, such a frequency limitation has minimal (if any) impact on the validity of the

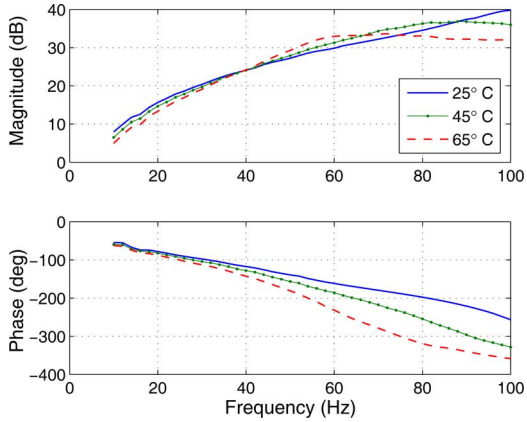

Fig. 5. Empirical frequency responses of an IPMC sensor under different temperatures. The input and output of the system are taken to be the IPMC tip displacement and the short-circuit current, respectively.

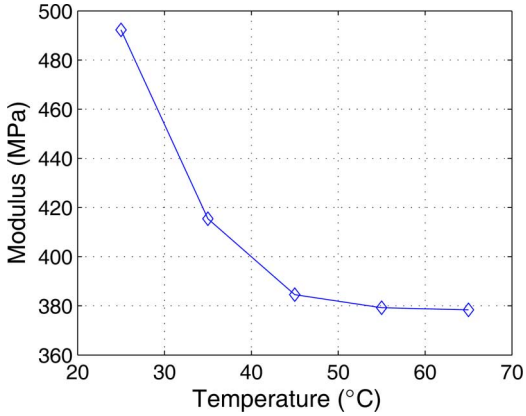

Fig. 6. Measured Young's modulus of IPMC versus the bath temperature.

proposed approach to modeling and inverse compensation of the temperature-dependent sensing behavior.

We measured the empirical frequency response of the sensor at different temperatures in the range of 23–65 °C. For each new temperature, sufficient time (more than 20 min) was allocated before taking the measurement, to let the IPMC sample sit in the bath so that its electrical, mechanical, and fluidic properties would have reached the steady state. The experiments were performed first with the temperature rising sequentially, and then with the temperature descending sequentially. No pronounced hysteresis was observed between the empirical frequency response of the sensor and the bath temperature.

Fig. 5 shows the measured frequency responses at three different bath temperatures: 25, 45, and 65 °C. In the figure, both the magnitude and phase responses show significant variation with temperature. If we view the sensor as a high-pass filter, it appears from the magnitude plot that, as the temperature increases, both the cutoff frequency and the high-frequency gain decrease. From the phase plot, the phase lag between the current output and the displacement input seems to increase consistently with the temperature.

The temperature-dependent sensing behavior, as observed in Fig. 5, can be attributed to a number of factors. For example, it is known that the water uptake of Nafion depends on the temperature, and the sensing behavior could vary with the amount of water uptake (or hydration) [31]. As another example, the stiffness of the IPMC is an important parameter in determining the sensing response, as shown in [31]. We measured the Young's modulus of the IPMC beam at different temperatures, using the experimental setup shown in [11, Fig. 5], and found that the Young's modulus depends nonlinearly on the temperature (see Fig. 6). Such dependence could be partly due to the water uptake factor, but other factors could play a role too. Besides water uptake and material stiffness, the ion diffusivity is yet another critical parameter of the sensing dynamics [12], [30], [31] that is heavily influenced by the temperature. Finally, the dielectric constant of IPMC, resistivity, and other electrical parameters are conceivably functions of the temperature. All the aforementioned factors could depend on the temperature in a nonlinear and complex way, and many of these variables are difficult to measure directly. Therefore, it would be a daunting task to provide a physical explanation of the specific trend observed in Fig. 5. Instead, using an empirical approach to model the temperature-dependent sensing dynamics becomes a natural alternative. As we will show later, such an approach will also lead to efficient algorithms for decoding the IPMC sensor signals under different temperatures.

III. Modeling of Temperature-Dependent Sensing Dynamics

For a given temperature, we used a linear time-invariant system to describe the IPMC sensing dynamics empirically. It was found that a fourth-order transfer function $G(s)$ could adequately approximate the measured frequency response for our sample, with

$$G(s) = \frac{b_4 s^4 + b_3 s^3 + b_2 s^2 + b_1 s + b_0}{s^4 + a_3 s^3 + a_2 s^2 + a_1 s + a_0}. \tag{1}$$

The coefficients $\{a_i\}_{i=0}^{3}$ and $\{b_i\}_{i=0}^{4}$ depend on the temperature. It is desirable to capture such a dependence with simple functions, so that the model at any temperature (within the studied range) can be obtained. To achieve this, we first identified the coefficients corresponding to a set of seven temperatures (23, 25, 30, 40, 50, 60, and 65 °C). For each of these temperatures, given the measured frequency response and the desired system order, we used the MATLAB command *invfreqs* to find the coefficients for the approximating transfer function $G(s)$. Then by fitting the values of each coefficient at different temperatures, we got a low-order polynomial function of the temperature T for that coefficient. For example, Fig. 7 shows the identified a_0 at different temperatures, along with the approximation by the polynomial function

$$a_0(T) = (4.81 - 0.043(T - 23.07) - 0.00028(T - 23.07)^2 + 8.56 \times 10^{-5}(T - 23.07)^3) \times 10^{10}.$$

To verify the prediction capability of the temperature-dependent model, we constructed the models at 35 and 45 °C based on (1) and the coefficient functions $\{a_i(T)\}_{i=0}^{3}$ and

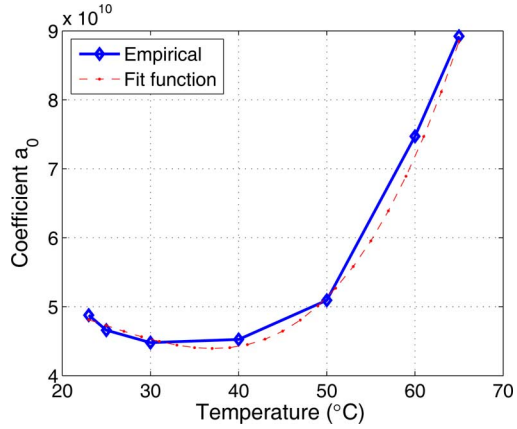

Fig. 7. Fitting function for coefficient a_0.

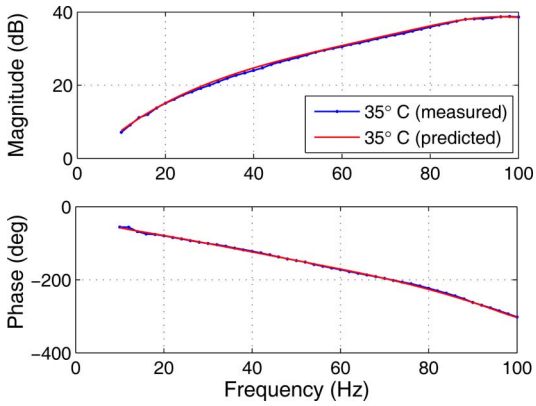

Fig. 8. Comparison of the measured frequency response and the model prediction at 35 °C. The input and output of the system are taken to be the IPMC tip displacement and the short-circuit current, respectively.

$\{b_i(T)\}_{i=0}^4$ evaluated at $T = 35$ and 45, respectively. Note that 35 and 45 °C were not used in data-fitting for obtaining the coefficient functions. Figs. 8 and 9 show the comparison between the measured frequency response and the predicted frequency response based on the models at these temperatures. The good agreement between the model prediction and the measurement in both figures shows that we can effectively predict the sensing dynamics at different temperatures.

IV. Inverse Compensation of Sensor Dynamics

A. Inverse Compensation Scheme

In applications, we need to infer the underlying mechanical signal given the output of an IPMC sensor. Let d and i denote the tip displacement and the current output of the sensor, respectively, and let $D(s)$ and $I(s)$ be their Laplace transforms. Then, $I(s) = G_T(s)D(s)$ with

$$G_T(s) = \frac{b_4(T)s^4 + b_3(T)s^3 + b_2(T)s^2 + b_1(T)s + b_0(T)}{s^4 + a_3(T)s^3 + a_2(T)s^2 + a_1(T)s + a_0(T)}. \tag{2}$$

Inferring $D(s)$ [or $d(t)$] requires the inversion of the sensing model $G_T(s)$; namely, $D(s) = (1/G_T(s))I(s)$. However, the models $G_T(s)$ we obtained are of nonminimum phase and the resulting $1/G_T(s)$ would be unstable and thus not implementable. For example, the model at 35 °C is

$$\frac{-17.3s^4 + 2.2 \times 10^4 s^3 - 10^7 s^2 - 9.4 \times 10^8 s + 4.5 \times 10^{10}}{s^4 + 835s^3 + 6.3 \times 10^5 s^2 + 2.5 \times 10^8 s + 4.4 \times 10^{10}}$$

which has one stable zero -106.7 and three unstable zeros: 35.2, $662.2 \pm 498.3j$. The nonminimum-phase property may have resulted from the fundamental sensing physics. Chen *et al.* derived an infinite-dimensional, physics-based dynamic model for IPMC sensors, and the corresponding reduced (finite-dimensional) model was of nonminimum phase [31].

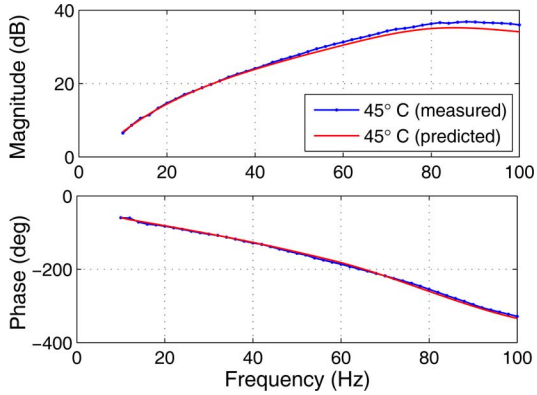

Fig. 9. Comparison of the measured frequency response and the model prediction at 45 °C. The input and output of the system are taken to be the IPMC tip displacement and the short-circuit current, respectively.

One alternative for circumventing the aforementioned problem could be identifying a stable transfer function model for the inverse dynamics directly based on the measurement data. In other words, one could take the IPMC sensing current as an input and the tip displacement as an output and seek a stable model for this relationship. However, despite our extensive search, there exist no stable inverse models that can provide reasonable match to the measured data.

In this paper, we explore the use of techniques for stable inversion of nonminimum-phase systems [33], [34] to obtain the IPMC tip displacement based on the sensing output. Let $G(s)$ be the forward sensor model, with input $D(s)$ and output $I(s)$. It is assumed that $G(s)$ is hyperbolic, implying that it has no zeros on the imaginary axis. The inversion problem is formulated as follows: given the sensor output function $i(t)$, $0 \le t < \infty$, find the function $d(t)$, $0 \le t < \infty$, such that

$$i(t) = G(s)[d](t) \tag{3}$$

where the mixed frequency–time domain notation $G(s)[d]$ represents the signal obtained by passing $d(\cdot)$ through the system $G(s)$. If $G(s)$ is a minimum-phase system, the solution $d(t)$ can be computed easily using

$$d(t) = H(s)[i](t) \tag{4}$$

with $H(s) = (1/G(s))$. For a nonminimum phase $G(s)$, as in the case of an IPMC sensor, $H(s)$ contains unstable poles and thus the algorithm (4) is not implementable. To solve the inversion problem, we decompose $H(s) = H_s(s) + H_u(s)$ where all poles of $H_s(s)$ have negative real parts (stable) while all poles

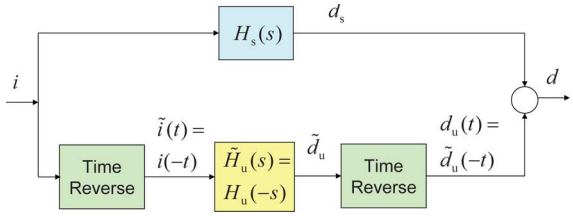

Fig. 10. Schematic of the inversion algorithm.

of $H_u(s)$ have positive real parts (unstable). Note that by the assumption on $G(s)$, $H(s)$ has no poles on the imaginary axis. The solution $d(t)$ to the inversion problem will correspondingly have two parts: $d(t) = d_s(t) + d_u(t)$, where $d_s(t) = H_s(s)[i](t)$ and $d_u(t)$ is computed as follows.

We first mirror the signal $i(t)$ with respect to $t = 0$ and obtain $\tilde{i}(t) = i(-t)$. Then, we pass the time-reversed signal $\tilde{i}$ through a stable system $\tilde{H}_u(s) \triangleq H_u(-s)$

$$\tilde{d}_u = \tilde{H}_u(s)[\tilde{i}](t).$$

We then obtain d_u from $\tilde{d}_u$ by reversing the time again, $d_u(t) = \tilde{d}_u(-t)$.

Fig. 10 illustrates the overall inversion algorithm. Note that evaluating $d_u(t^*)$ [or equivalently, $\tilde{d}_u(-t^*)$], for some t^*, requires knowing $\tilde{i}(t')$, for all $t' < -t^*$, or equivalently, $i(t)$, for all $t > t^*$. Therefore, the essence of stable inversion of a nonminimum-phase system lies in converting an originally stable but causal system to a stable but noncausal system.

B. Experimental Results

In Fig. 11, we compare the displacement trajectory measured by the laser sensor with that predicted by the inverse compensator based on the IPMC sensor output, where the bath temperature was 50 °C. In the experiment, a sinusoidal mechanical stimulus was applied at 25 Hz. The top panel shows the measured IPMC sensing current, the middle panel compares the measured and predicted tip displacement trajectories, and the bottom panel shows the prediction error. Figs. 12 and 13 show the results when the bath temperature was 35 °C with the mechanical stimulus applied at 20 and 54 Hz, respectively. It can be seen that, for different bath temperatures and stimulus frequencies, the predicted and actual displacement trajectories have always achieved excellent agreement, indicating that the modeling and inverse compensation schemes are effective.

We have also experimented with a different type of mechanical stimuli. Instead of using the forced oscillation with the speaker system, we first displace the IPMC beam tip and hold it still, and then let it go. The beam will go through free, damped oscillations. Figs. 14 and 15 show the results when the bath temperatures were 50 and 35 °C, respectively. The top panel in each figure shows the measured IPMC sensing current while the bottom panel shows the measured and predicted tip displacements. In both cases, the measured and predicted displacements have good agreement following the first peak; in particular, the prediction has captured well both the decay and the oscillation frequency. However, there is big mismatch around the time when

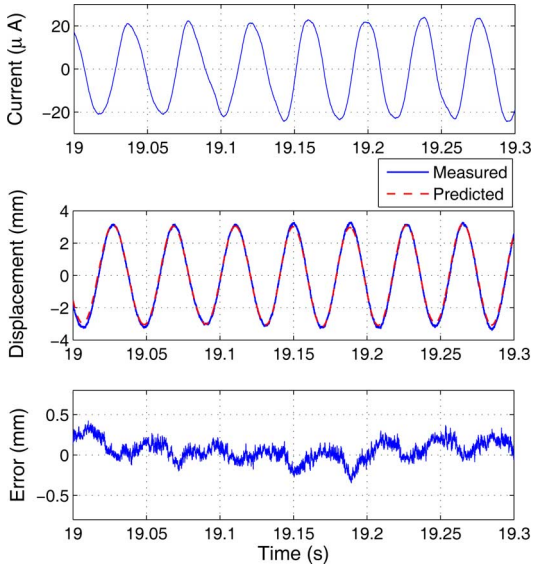

Fig. 11. Comparison of displacement obtained through model-based inverse compensation with that measured by a laser sensor (25 Hz, 50 °C).

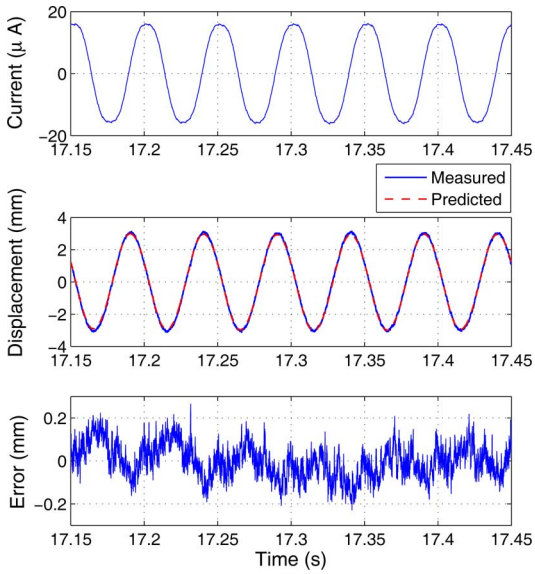

Fig. 12. Comparison of displacement obtained through model-based inverse compensation with that measured by a laser sensor (20 Hz, 35 °C).

the beam is released. There could be two causes for this. First, the sensor dynamics could be slightly different from the modeled case because of the holding process (blocking force applied). Second, stable but noncausal implementation of the inversion algorithm could result in some nonzero trajectory even prior to the moment the beam was released, which is analogous to the "preactuation" effect in the context of inversion-based output tracking control [33]. The exact cause of the mismatch during the transients is still under investigation.

V. Inverse Compensation With Finite Preview Time

The algorithm introduced in Section IV-A is noncausal. In particular, to evaluate the value of d_u at any time t^*, one needs

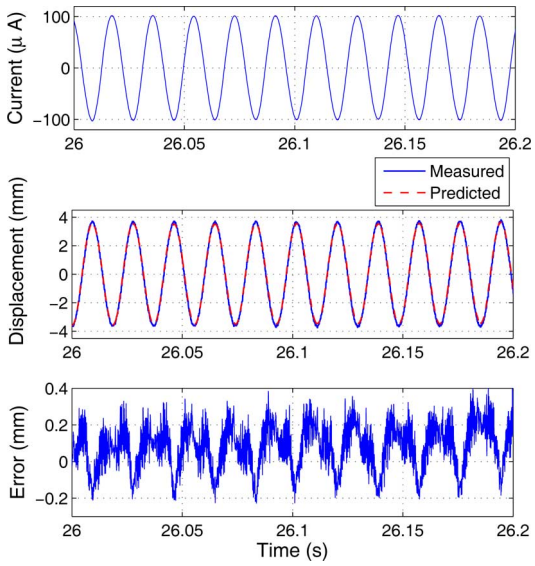

Fig. 13. Comparison of displacement obtained through model-based inverse compensation with that measured by a laser sensor (54 Hz, 35 °C).

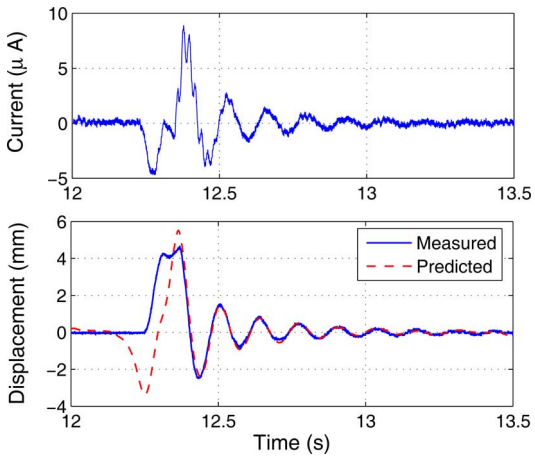

Fig. 14. Predicted free vibration versus experimental measurement (50 °C).

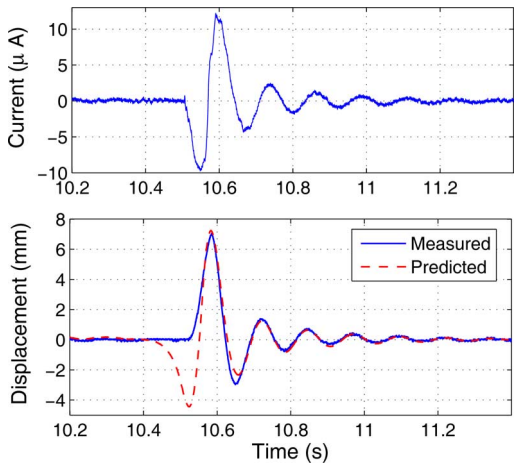

Fig. 15. Predicted free vibration versus experimental measurement (35 °C).

to know the trajectory of the current output $i(t)$ for all $t > t^*$. In other words, the algorithm would only be useful for the postprocessing of the sensor data. In many applications, it is desirable to extract the mechanical stimulus information in near real time. For this purpose, we examine inverse compensation with finite preview (or look-ahead) time.

In order to explain the algorithm with finite preview time, we first rewrite the computation in the lower branch of Fig. 10 in the time domain. Let $(A_{\rm u}, B_{\rm u}, C_{\rm u})$ be a minimal state-space realization of the unstable system $H_{\rm u}(s)$

$$\dot{x}_{\rm u}(t) = A_{\rm u} x_{\rm u}(t) + B_{\rm u} u(t)$$
$$y(t) = C_{\rm u} x_{\rm u}(t)$$

where $x_{\rm u}$, $A_{\rm u}$, $B_{\rm u}$, and $C_{\rm u}$ have appropriate dimensions, and u and y denote the scalar input and output, respectively. We can then write

$$\begin{aligned} d_{\rm u}(t) &= \tilde{d}_{\rm u}(-t) \\ &= H_{\rm u}(-s)\,[\tilde{i}\,](-t) \\ &= -C_{\rm u} \int_{-\infty}^{-t} e^{-A_{\rm u}(-t-\theta)}\, B_{\rm u}\, \tilde{i}(\theta)\, d\theta \\ &= -C_{\rm u} \int_{t}^{\infty} e^{-A_{\rm u}(t'-t)}\, B_{\rm u}\, \tilde{i}(-t')\, dt' \\ &= -C_{\rm u} \int_{t}^{\infty} e^{-A_{\rm u}(t'-t)}\, B_{\rm u}\, i(t')\, dt'. \end{aligned} \tag{5}$$

It is evident from (5) that the evaluation of $d_{\rm u}(t)$ requires knowing $i(t')$, $t' > t$. In the finite preview-based algorithm, the upper limit of integration in (5) is changed to $t + T_p$ for some finite preview time $T_p > 0$. In other words, an approximation $\bar{d}(t)$ to $d(t)$ is obtained as

$$\bar{d}(t) = -C_{\rm u} \int_{t}^{t+T_p} e^{-A_{\rm u}(t'-t)}\, B_{\rm u}\, i(t')\, dt'. \tag{6}$$

An important question is how to pick a small T_p so that the finite preview-based estimate $\bar{d}$ is sufficiently close to d. Based on the work of Zou and Devasia [34], a sound choice τ^* of T_p is related to the real part r_0 of the least unstable pole (i.e., the pole closest to the imaginary axis) of $H_{\rm u}(s)$. In particular, $\tau^* = (4/r_0)$. This can be understood as follows. Since $(1/r_0)$ also represents the time constant [37] τ_0 of the stable system $H_{\rm u}(-s)$, the influence of $i(t)$ from $\tau^* = 4\tau_0$ seconds away on the inversion output is negligible.

We now validate the analysis with an example where the bath temperature is 35 °C. From the discussion in Section IV-A, $r_0 = 35.2$, and the corresponding $\tau^* = 0.114$ s. Fig. 16 shows the comparison of the model-predicted displacement trajectory with the actual measurement for the bath temperature of 35 °C, where we have used a finite preview time of τ^*. The trajectory of IPMC sensor signal, which is used as the input to the inverse compensation, is the same as in Fig. 12 and is thus not shown here. From Fig. 12, the performance of the inversion with preview of τ^* seconds is comparable to the case with infinite preview time, and in both cases the largest error is around 0.2 mm. On the other hand, if we reduce T_p to one half of τ^*,

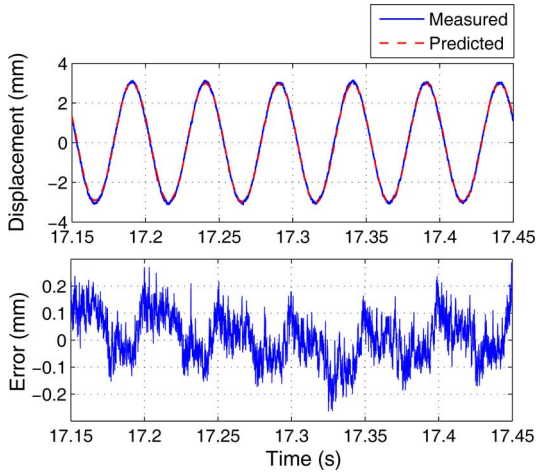

Fig. 16. Inverse compensation with finite preview time $T_p = \tau^*$ (20 Hz, 35 °C).

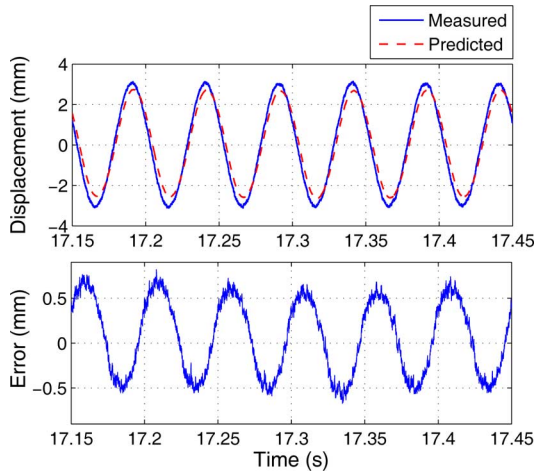

Fig. 17. Inverse compensation with finite preview time $T_p = 0.5\tau^*$ (20 Hz, 35 °C).

there is a threefold increase in the prediction error, as is seen in Fig. 17. This indicates that τ^* indeed provides a good choice for the finite preview time T_p.

VI. Conclusion

In this paper, we have characterized the temperature dependence of IPMC sensor dynamics and proposed an empirical modeling approach for capturing such a dependence. The model takes the form of a linear time-invariant system with temperature-dependent parameters via simple, polynomial functions. In practice, an auxiliary measurement of temperature will be used to determine the model parameters. An inverse compensation scheme has been further presented for extracting the mechanical stimulus given the sensor output. Since the sensor model has unstable zeros, direct inversion is not feasible. The proposed scheme implements the inversion in a stable but noncausal way. To reduce the processing delay, we have explored the inversion with a finite preview time. Experimental results, with sinusoidal and free-vibration mechanical stimuli, have confirmed that the modeling and inverse compensation approach is effective.

Note that the main contribution of this paper is the proposed *methodology* for capturing and compensating the temperature-dependent dynamics of IPMC sensors, and the quantitative results obtained for the specific sample used in the study are of less relevance. Because of the empirical nature of the approach, the model structure (e.g., the order of the model), model parameters, and parameter–temperature relationships could vary with materials, operational frequency range, and sample dimensions. For example, the experimental characterization of the temperature-dependent behavior was limited to 10–100 Hz and the resulting model may not necessarily capture well the response under a step stimulus. However, the general idea of how to model and accommodate the temperature dependence as presented in this paper is expected to work under those and other different scenarios. In addition, the presented approach can potentially be used for other classes of electroactive polymer sensors, such as conjugated polymer sensors [38], [39], where the temperature could impact various electrical, mechanical, and chemical properties of the material.

Future work will involve the application of the proposed approach to modeling and compensating the temperature-dependent behavior for IPMC actuators, which has been confirmed in our preliminary work. We will also examine the use of the proposed methodology in real applications, such as flow sensing and tactile sensing, where the ambient temperature could be time varying.

References

[1] Y. Bar-Cohen, *Electroactive Polymer Actuators as Artificial Muscles: Reality, Potential and Challenges*. Bellingham, WA: SPIE, 2001.
[2] M. Shahinpoor and K. Kim, "Ionic polymer-metal composites: I. Fundamentals," *Smart Mater. Struct.*, vol. 10, pp. 819–833, 2001.
[3] E. Smela, "Conjugated polymers for biomedical applications," *Adv. Mater.*, vol. 15, no. 6, pp. 481–494, 2003.
[4] G. G. Wallace, G. M. Spinks, L. Kane-Maguire, and P. R. Teasdale, *Conductive Electroactive Polymers: Intelligent Materials Systems*, 2nd ed. Boca Raton, FL: CRC Press, 2003.
[5] Y. Fang, X. Tan, Y. Shen, N. Xi, and G. Alici, "A scalable model for trilayer conjugated polymer actuators and its experimental validation," *Mater. Sci. Eng.: C*, vol. 28, no. 3, pp. 421–428, 2008.
[6] Y. Fang, X. Tan, and G. Alici, "Robust adaptive control of conjugated polymer actuators," *IEEE Trans. Control Syst. Technol.*, vol. 16, no. 4, pp. 600–612, Jul. 2008.
[7] Y. Fang, T. J. Pence, and X. Tan, "Fiber-directed conjugated polymer torsional actuator: Nonlinear elasticity modeling and experimental validation," *IEEE/ASME Trans. Mechatronics*, vol. PP, no. 99, pp. 1–9, Jun. 2010.
[8] Y. Fang and X. Tan, "A novel diaphragm micropump actuated by conjugated polymer petals: Fabrication, modelling, and experimental results," *Sens. Actuators A: Physical*, vol. 158, pp. 121–131, 2010.
[9] F. Carpi, C. Salaris, and D. De Rossi, "Folded dielectric elastomer actuators," *Smart Mater. Struct.*, vol. 16, pp. S300–S305, 2007.
[10] K. Jung, J. Lee, M. Cho, J. C. Koo, J. Nam, Y. Lee, and H. R. Choi, "Development of enhanced synthetic elastomer for energy-efficient polymer actuators," *Smart Mater. Struct.*, vol. 16, pp. S288–S294, 2007.
[11] Z. Chen and X. Tan, "Monolithic fabrication of ionic polymer-metal composite actuators capable of complex deformation," *Sens. Actuators A: Physical*, vol. 157, pp. 246–257, 2010.
[12] S. Nemat-Nasser and J. Li, "Electromechanical response of ionic polymer-metal composites," *J. Appl. Phys.*, vol. 87, no. 7, pp. 3321–3331, 2000.
[13] Z. Chen and X. Tan, "A control-oriented and physics-based model for ionic polymer-metal composite actuators," *IEEE/ASME Trans. Mechatronics*, vol. 13, no. 5, pp. 519–529, Oct. 2008.

[14] M. Shahinpoor and K. Kim, "Ionic polymer-metal composites: IV. Industrial and medical applications," *Smart Mater. Struct.*, vol. 14, pp. 197–214, 2005.
[15] Z. Chen, S. Shatara, and X. Tan, "Modeling of biomimetic robotic fish propelled by an ionic polymer-metal composite caudal fin," *IEEE/ASME Trans. Mechatronics*, vol. 15, no. 3, pp. 448–459, Jun. 2010.
[16] S. D. Peterson, M. Porfiri, and A. Rovardi, "A particle image velocimetry study of vibrating ionic polymer metal composites in aqueous environments," *IEEE/ASME Trans. Mechatronics*, vol. 14, no. 4, pp. 474–483, Aug. 2009.
[17] M. Aureli, V. Kopman, and M. Porfiri, "Free-locomotion of underwater vehicles actuated by ionic polymer metal composites," *IEEE/ASME Trans. Mechatronics*, vol. 15, no. 4, pp. 603–614, Aug. 2010.
[18] M. Mojarrad and M. Shahinpoor, "Ion-exchange-metal composite sensor films," in *Smart Structures and Materials 1997: Smart Sensing, Processing, and Instrumentation*, vol. 3042, R. O. Claus, Ed. Bellingham, WA: SPIE, 1997, pp. 52–60.
[19] L. Ferrara, M. Shahinpoor, K. J. Kim, H. B. Schreyer, A. Keshavarzi, E. Benzel, and J. W. Lantz, "Use of ionic polymer-metal composites (IPMCs) as a pressure transducer in the human spine," in *Smart Structures and Materials 1999: Electroactive Polymer Actuators and Devices*, Y. Bar-Cohen, Ed. Bellingham, WA: SPIE, 1999, pp. 394–401.
[20] A. Keshavarzi, M. Shahinpoor, K. J. Kim, and J. W. Lantz, "Blood pressure, pulse rate, and rhythm measurement using ionic polymer-metal composite sensors," in *Smart Structures and Materials 1999: Electroactive Polymer Actuators and Devices*, vol. 3669, J. Bar-Cohen, Ed. Bellingham, WA: SPIE, 1999, pp. 369–376.
[21] M. Konyo, Y. Konishi, S. Tadokoro, and T. Kishima, "Development of velocity sensor using ionic polymer-metal composites," in *Smart Structures and Materials 2004: Electroactive Polymer Actuators and Devices*, J. Bar-Cohen, Ed. Bellingham, WA: SPIE, 2004, pp. 307–318.
[22] C. Bonomo, L. Fortuna, P. Giannone, and S. Graziani, "A sensor-actuator integrated system based on IPMCs," in *Proc. IEEE Sensors*, 2004, pp. 489–492.
[23] E. Biddiss and T. Chau, "Electroactive polymeric sensors in hand prostheses: Bending response of an ionic polymer metal composite," *Med. Eng. Phys.*, vol. 28, pp. 568–578, 2006.
[24] C. Bonomo, P. Brunetto, L. Fortuna, P. Giannone, S. Graziani, and S. Strazzeri, "A tactile sensor for biomedical applications based on IPMCs," *IEEE Sens. J.*, vol. 8, no. 8, pp. 1486–1493, Aug. 2008.
[25] D. Pugal, K. Jung, A. Aabloo, and K. J. Kim, "Ionic polymer-metal composite mechanoelectrical transduction: Review and perspectives," *Polymer Int.*, vol. 59, pp. 279–289, 2010.
[26] P. G. de Gennes, K. Okumura, M. Shahinpoor, and K. Kim, "Mechanoelectric effects in ionic gels," *Europhys. Lett.*, vol. 50, no. 4, pp. 513–518, 2000.
[27] K. M. Newbury and D. J. Leo, "Electromechanical modeling and characterization of ionic polymer benders," *J. Intell. Mater. Syst. Struct.*, vol. 13, pp. 51–60, 2002.
[28] K. Newbury, "Characterization, modeling, and control of ionic polymer transducers," Ph.D. dissertation, Dept. Mech. Eng., Virginia Polytechnic Institute and State University, Blacksburg, 2002.
[29] C. Bonomo, L. Fortuna, P. Giannone, S. Graziani, and S. Strazzeri, "A model for ionic polymer metal composites as sensors," *Smart Mater. Struct.*, vol. 15, pp. 749–758, 2006.
[30] K. Farinholt and D. Leo, "Modeling of electromechanical charge sensing in ionic polymer transducers," *Mech. Mater.*, vol. 36, pp. 421–433, 2004.
[31] Z. Chen, X. Tan, A. Will, and C. Ziel, "A dynamic model for ionic polymer-metal composite sensors," *Smart Mater. Struct.*, vol. 16, pp. 1477–1488, 2007.
[32] K. Takagi, N. Kamamichi, B. Stoimenov, K. Asaka, T. Mukai, and Z.-W. Luo, "Frequency response characteristics of IPMC sensors with current/voltage measurements," in *Electroactive Polymer Actuators and Devices (EAPAD)* (ser. Proceedings of SPIE), vol. 6927, Y. Bar-Cohen, Ed. Bellingham, WA: SPIE, 2008, pp. 692 724:1–10.
[33] S. Devasia, D. Chen, and B. Paden, "Nonlinear inversion-based output tracking," *IEEE Trans. Autom. Control*, vol. 41, no. 7, pp. 930–942, Jul. 1996.
[34] Q. Zou and S. Devasia, "Preview-based optimal inversion for output tracking: Application to scanning tunneling microscopy," *IEEE Trans. Control Syst. Technol.*, vol. 12, no. 3, pp. 375–386, May 2004.
[35] K. J. Kim and M. Shahinpoor, "Ionic polymer-metal composites: II. Manufacturing techniques," *Smart Mater. Struct.*, vol. 12, no. 1, pp. 65–79, 2003.
[36] S. J. Kim, I. T. Lee, and Y. H. Kim, "Performance enhancement of IPMC actuator by plasma surface treatment," *Smart Mater. Struct.*, vol. 16, no. 1, pp. N6–N11, 2007.
[37] N. S. Nise, *Control Syst. Eng.*, 4th ed. Hoboken, NJ: Wiley, 2004.
[38] Y. Fang, X. Tan, A. Temme, and G. Alici, "Characterization and modeling of conjugated polymer sensors," in *Electroactive Polymer Actuators and Devices (EAPAD)* (ser. Proceedings of SPIE), vol. 6927, Y. Bar-Cohen, Ed. Bellingham, WA: SPIE, 2008, pp. 692 709:1–692 709:9.
[39] G. Alici, G. M. Spinks, J. D. Madden, Y. Wu, and G. G. Wallace, "Response characterization of electroactive polymers as mechanical sensors," *IEEE/ASME Trans. Mechatronics*, vol. 13, no. 2, pp. 187–196, Apr. 2008.

Tom Ganley is currently working toward the B.S. degree in electrical engineering at Michigan State University (MSU), East Lansing . Upon graduation, he will be joining a full-time rotational program at General Electric while pursuing the M.S. degree in electrical engineering.

He was a Research Assistant in the Smart Microsystems Laboratory, MSU, where he conducted research on ionic polymer–metal composite sensors.

Mr. Ganley is an active member and the Public Relations Chair of the IEEE Michigan State University Chapter.

David L. S. Hung received the B.S. degree with distinction in mechanical engineering from Iowa State University, Ames, in 1991, and the M.Eng. and Ph.D. degrees in mechanical engineering from Carnegie Mellon University, Pittsburgh, PA, in 1993 and 1998, respectively.

He is currently an Associate Professor of Mechanical Engineering at the University of Michigan-Shanghai Jiao Tong University Joint Institute (UM-SJTU JI), Shanghai, China. He is also appointed as a Professor in the School of Mechanical Engineering at Shanghai Jiao Tong University. Previously, he was an Associate Professor in the Department of Mechanical Engineering, Michigan State University, East Lansing. Between 1998 and 2009, he also held positions in the automotive industry at General Motors, Delphi, and Visteon, where he was responsible for developing gasoline direct injection systems and optical diagnostics for in-cylinder fuel mixture preparation and combustion measurements. His research interests include the development and utilization of sustainable energy systems, renewable fuels for vehicle and aviation applications, and optical diagnostics and novel flow sensing techniques.

Dr. Hung is active in various technical organizations such as the Society of Automotive Engineers (SAE), Institute of Liquid Atomization and Spray Systems, and Aviation Technical Committee of Coordinating Research Council . He is leading a task force for the SAE Gasoline Fuel Injection Standards Committee that includes an industry-wide team of automotive fuel system and spray measurement experts to develop and improve new and existing engineering standards. He has received four SAE International awards, including the 2007 Henry Souther Standards Award and the 2009 SAE/interregs Standards and Regulations Award for Young Engineers, for his contributions to developing global engineering standards and regulations for the global automotive industry.

Guoming (George) Zhu received the B.S. and M.S. degrees from Beijing University of Aeronautics and Astronautics, Beijing, China, in 1982 and 1984, respectively, and the Ph.D. degree in aerospace engineering from Purdue University, West Lafayette, IN, in 1992.

He is an Associate Professor in the Department of Mechanical Engineering (ME), Michigan State University, East Lansing. Prior to joining the ME Department, he was a Technical Fellow in Advanced Powertrain Systems of Visteon Corporation, Van Buren Twp, MI. He also worked for Cummins Engine Company, Columbus, IN. He has more than 24 years of experience related to control theory, engine diagnostics, and combustion control. He is the author or coauthor of more than 90 refereed technical papers and has received 38 U.S. patents. His teaching interests focus on control classes at both undergraduate and graduate levels, and his current research interests include closed-loop combustion control of internal combustion engines, engine system modeling and identification, and hybrid powertrain control and optimization.

Dr. Zhu is an Associate Editor of the *ASME Journal of Dynamic Systems, Measurement, and Control*.

Xiaobo Tan (S'97–M'02) received the B.Eng. and M.Eng. degrees in automatic control from Tsinghua University, Beijing, China, in 1995 and 1998, respectively, and the Ph.D. degree in electrical and computer engineering from the University of Maryland, College Park, in 2002.

From September 2002 to July 2004, he was a Research Associate at the Institute for Systems Research, University of Maryland. In August 2004, he joined the Department of Electrical and Computer Engineering, Michigan State University (MSU), East Lansing, as an Assistant Professor, and founded the Smart Microsystems Laboratory. Since July 2010, he has been an Associate Professor at MSU . He is keen to integrate his research with educational and outreach activities, and currently leads a National Science Foundation (NSF) funded Research Experiences for Teachers Site on Bio-Inspired Technology and Systems, MSU. His current research interests include electroactive polymer sensors and actuators, biomimetic robotic fish, mobile sensing in aquatic environments, modeling and control of smart materials, and collaborative control of autonomous systems.

Dr. Tan is an Associate Editor of *Automatica* and is serving as the Program Chair for the 15th International Conference on Advanced Robotics in 2011). He was a Guest Editor of *IEEE Control Systems Magazine* for its February 2009 issue's Special Section on Modeling and Control of Hysteresis. He received an NSF CAREER Award in 2006, the 2008 ASME Dynamic Systems and Control Division Best Mechatronics Paper Award (with Yang Fang) in 2009, and the Teacher–Scholar Award from MSU in 2010.